

# On the Benefits of Attributional Robustness

Mayank Singh\*  
Adobe Inc, Noida, India  
msingh@adobe.com

Nupur Kumari\*  
Adobe Inc, Noida, India  
nupkumar@adobe.com

Puneet Mangla  
IIT Hyderabad, India  
cs17btech11029@iith.ac.in

Abhishek Sinha  
Work done at Adobe  
abhishek.sinha94@gmail.com

Vineeth N Balasubramanian  
IIT Hyderabad, India  
vineethnb@iith.ac.in

Balaji Krishnamurthy  
Adobe Inc, Noida, India  
kbalaji@adobe.com

## Abstract

*Interpretability is an emerging area of research in trustworthy machine learning. Safe deployment of machine learning system mandates that the prediction and its explanation be reliable and robust. Recently, it was shown that one could craft perturbations that produce perceptually indistinguishable inputs having the same prediction, yet very different interpretations. We tackle the problem of attributional robustness (i.e. models having robust explanations) by maximizing the alignment between the input image and its saliency map using soft-margin triplet loss. We propose a robust attribution training methodology that beats the state-of-the-art attributional robustness measure by a margin of  $\approx 6-18\%$  on several standard datasets, ie. SVHN, CIFAR-10 and GTSRB. We further show the utility of the proposed robust model in the domain of weakly supervised object localization and segmentation. Our proposed robust model also achieves a new state-of-the-art object localization accuracy on the CUB-200 dataset.*

## 1. Introduction

Application of machine learning algorithms in various safety-critical domains is being hindered due to the black-box nature of these techniques. Robustness and interpretability of machine learning methods has become a crucial topic and a pre-requisite for successful deployment in various fields (e.g. self-driving cars, medical diagnosis). Hence, the field of explanation is attracting a lot of attention as it offers insight into decision making procedure of machine learning techniques. Attribution/saliency methods are an increasingly popular class of explanation techniques that aim to highlight relevant input features responsible for prediction.

\* Authors contributed equally



Figure 1: Illustration of an attributional attack [18]; Top row: original image and its attribution map; Bottom row: perturbed image and its attribution map [59]

Most deep learning research in the area of robustness is focused around the robustness to adversarial perturbations [24, 60]. Adversarial perturbations are imperceptible perturbation when added to input drastically change the neural network’s prediction. In contrast, in this paper, we focus on another type of robustness measure for neural networks which we refer to as attributional robustness. Recently, [23, 18] demonstrated that one can generate minimal perturbations that can substantially change the model’s interpretations, while keeping the predictions intact. Unfortunately, while the area of adversarial robustness is well studied, there has only been limited progress made on the front of attributional robustness.

We show in figure 1 the vulnerability of image classifiers to attribution based attacks. The intuition of attributional robustness is that if the prediction and input of model remains intact, then so should the interpretation. It has been demonstrated that one can construct targeted [18] and un-targeted attributional perturbations [23, 14] that can manipulate the

amount of changes induced in the attribution maps without affecting the model’s prediction. This is a particularly alarming issue as it further weakens the cause of safe application of machine learning algorithms to real world tasks.

The authors of [14] propose a training methodology that aims to obtain models having robust integrated gradient [59] attributions. However, sometimes the instability of this training methodology as discussed in [14] limits its usability in the broader context of robust attribution in computer vision. In this paper, we introduce a training technique that achieves state-of-the-art attributional robustness across different attribution methods [53, 59] and also show its utility in the domain of weakly supervised object detection and segmentation.

Specifically, we introduce a training methodology for attributional robustness that uses soft-margin triplet loss to promote the alignment of an input with its attribution map. The triplet loss considers the input image as the anchor, the gradient of the correct class logit with respect to input as the positive and the gradient of the worst incorrect class logit with respect to input as the negative. The intuition behind this loss choice is that the gradient of the correct class logit with respect to input should have the highest similarity with input as compared to gradient of any other class logit with respect to input. We show empirically how this choice results in attributional robustness of neural network and helps in other weakly supervised tasks.

To summarize our main contributions are:

- We introduce the concept of attributional robustness and highlight the significance of it as a general measure that helps broaden the notion of robustness for neural networks.
- We propose a robust attribution training methodology that aims to maximize the alignment between the input and its attribution map [53]. The proposed model training technique achieves state-of-the-art attributional robustness on various saliency methods.
- We empirically show that the proposed training methodology also induces significant immunity to adversarial perturbations and common perturbations on standard vision datasets.
- We demonstrate the utility of our proposed attributional training approach for other computer vision tasks such as weakly supervised object localization and segmentation. Specifically, our proposed model achieves the new state-of-the-art result in weakly supervised object localization on CUB dataset using attributional robustness.

## 2. Related Work

Our work is associated with various recent development made in the field of reliable explanation methods, weakly supervised object localization and robustness to input distribution shifts.

**Visual Explanation Methods** Various explanation methods have been proposed that focus on producing posterior explanations for the model’s decisions. A popular approach to do so is to attribute the predictions to the set of input features [53, 57, 52, 59, 51, 8] that can be referred to as attribution or saliency methods. Sample-based explanation methods [32, 70] leverage previously seen examples to describe the prediction of the model. Concept-based explanation techniques [9, 31] aim to explain the decision of the model by high-level concepts. Additionally, there has been some work that explores interpretability as a built-in property of architecture inspired by the characteristics of linear models [6]. [78, 19] provide a survey of interpretation techniques. In this paper, we will be focusing on attribution-based methods that generate visual, image-like explanations. Attribution methods can be broadly divided into three categories - gradient/back-propagation, activation and perturbation based methods.

Gradient based methods attribute an importance score for each pixel by calculating derivative of a class score with respect to input image pixels [53, 52]. Further improvements have been proposed in which gradients are accumulated along a path from a reference image to input image [59], or by only considering the gradients through positive activation while back-propagating [73, 57] or by aggregating gradients on multiple noisy images of the original image to obtain attribution maps [56, 1]. Techniques in [8, 51, 76] leverage layer-wise propagation computation to calculate the attribution maps. Activation based explanation techniques generate the attribution maps by using a weighed linear combination of the convolutional’s activation. [82, 50, 13]. Perturbation based interpretation methods generate attribution maps by examining the change in prediction of the model when the input image is perturbed [73, 46, 48]. Related to this, similar methods [17, 22, 66, 12] generate an explanation by optimizing for a perturbed version of the image.

**Robustness of Attribution maps** Recently, several research work [79, 23, 18, 14, 5] has been exploring the robustness of attribution maps, that we refer to as attributional robustness. The authors of [23, 18, 79] study the robustness of a network’s attribution maps and show that these saliency maps can be significantly manipulated via imperceptible input perturbations while preserving the classifier’s prediction. [14] proposes a robust attribution training methodol-

ogy, that minimizes the norm of integrated gradients [59] to achieve attributional robustness with respect to integrated gradients explanation. The method introduced in [14] is the current state-of-the-art training procedure in the area of attributional robustness.

The authors of [2] present a list of sanity checks for assessing attribution method’s faithfulness to the model and it’s training data. They propose model parameter randomization test and the data randomization test as an evaluation criteria to suggest that method’s visual inspection alone is not sufficient. We stress here that our work is orthogonal to this, as we focus on the fragility of model’s attribution map derived by different saliency maps and not on the fragility and assessment of a particular explanation technique.

**Adversarial Perturbation** Adversarial attacks can be broadly categorized into two types: White-box [39, 37, 11, 69] and Black-box attacks [28, 63, 4, 45]. White-box attack assumes full access to the network while in the latter, information about the network is not available. Defense strategies to improve the adversarial robustness of deep networks include the use of regularizers inspired by reducing the Lipschitz constant of the neural network [62, 16]. However, many of proposed defense techniques were shown to be ineffective to adaptive adversarial attacks [7, 35, 11, 10]. Hence, we focus on adversarial training which [25, 37, 55] is a defense technique that continuously augments the data with adversarial examples while training. Techniques relying on adversarial training constitutes the current state-of-the-art in adversarial robustness. The authors of [75] characterize the trade-off between accuracy and robustness for classification problems and propose a regularized adversarial training method. Recent work of [47] proposes a regularizer that encourages the loss to behave linearly in the vicinity of the training data and [74] improves the adversarial training by also minimizing the convolutional feature distance between the perturbed and clean examples. Prior works have also attempted to improve the adversarial robustness using gradient regularization that minimizes the Frobenius norm of the Hessian of the classification loss with respect to input [49, 40, 36] or weights [29]. In the context of this paper we will mainly focus on perturbations of  $l_{inf}$  norm bound rather than other constraint bounds [68, 20]. For a comprehensive review of the work done in the area of adversarial examples, please refer [71, 3].

**Weakly Supervised Object Localization (WSOL)** The problem of WSOL aims to identify the location of the object in a scene using only the image-level labels, and without any location annotations. Generally, rich labeled data is scarcely available and it’s collection is expensive and time consuming. Therefore, the field of learning from weak su-

pervision is quite promising as it requires less rich labels and thus has the potential to scale. A common problem with most of the previous approaches is that the model only identifies the most discriminative part of the object rather than the complete object. For example, in the case of a bird, the model may rely on the beak region for classification than the entire bird’s shape. In WSOL task, ADL [15] is the current state-of-the-art method that uses an attention based dropout layer while training the model that promotes the classification model to also focus on less discriminative parts of the image. For getting the bounding box from the model, ADL and similar other techniques in this domain first extract attribution map, generally CAM [82], for each image and then fit a bounding box on this as presented in [82].

### 3. Methodology

We consider a neural network  $f_{\theta} : \mathbb{R}^n \rightarrow \mathbb{R}^k$  with relu activation functions which classifies an input image  $x \in [0, 1]^n$  into  $k$  classes with true label  $y \in \{1 \dots k\}$ . The logit value corresponding to class  $i \in \{1 \dots k\}$  is denoted as  $f(x)_i$ . For a given class  $i$ , attribution map is referred as  $I(x, f(x)_i)$  that assigns an importance score to each input pixel of  $x$  based on its relevance for predicting the class  $i$ .

#### 3.1. Attributional Robustness

We define a classification model  $f_{\theta}$  to be attributionally robust if the attribution maps do not change drastically with slight perturbation to inputs. The objective of attributional robustness is to ensure that similar feature importance is assigned to pixels for visually similar images.

**Attributional Attack** Attributional robustness measures the maximum possible change in attribution map on applying a small norm bounded perturbation  $\delta$  to  $x$  over the dataset. The problem of calculating  $\delta$  can be formulated as

$$\begin{aligned} & \arg \max_{\delta \in B_{\epsilon}} D[I(x + \delta, f(x + \delta)_y), I(x, f(x)_y)] \\ & \text{subject to: } \arg \max(f(x)) = \arg \max(f(x + \delta)) = y \end{aligned} \tag{1}$$

where  $B_{\epsilon}$  is an  $\epsilon$  ball under  $p$  norm which bounds the norm of  $\delta$  with which input  $x$  can be perturbed and  $D$  measures distance/dissimilarity between two attribution maps.

After obtaining  $\delta$ , we calculate similarity (e.g. using spearman correlatin [23], kendall’s tau coefficient [14]) between attribution map of original image  $x$ , and perturbed image  $x + \delta$ , to get a measure of attributional robustness in the  $\epsilon$  neighbourhood of sample  $x$ . Taking an expectation over the validation set of data gives us an approximate empirical measure of the attributional robustness of the network for a particular dataset. Some examples of dissimilarity measures for calculating  $\delta$  have been proposed in

---

**Algorithm 1** Proposed training for attributional robustness

---

**begin****Input:** Training Data  $X = \{(x_1, y_1) \dots (x_N, y_N)\}$ , batch size  $b$ , number of epochs  $E$ , learning rate  $lr$ , number of attack steps  $a$ , step-size for iterative perturbation  $\alpha$ **Output:**  $f_\theta$ Initialize variables  $\theta$ **for**  $epoch \in \{1, 2, \dots, E\}$  **do**    Get mini-batch  $x, y = \{(x_1, y_1) \dots (x_b, y_b)\}$      $\tilde{x} = x + \text{Uniform}[-\epsilon, +\epsilon]$     **for**  $i=1, 2, \dots, a$  **do**         $\tilde{x} = \tilde{x} + \alpha * \text{sign}(\nabla_x L_{attr}(\tilde{x}, y))$          $\tilde{x} = \text{Proj}_{l_\infty}(\tilde{x})$     **end**     $i^* = \text{ground truth index}$      $j^* = \arg \max_{j \neq i} \text{logit}_j$     Calculate  $g_1 = \nabla_x (f(\tilde{x})_{i^*})$     Calculate  $g_2 = \nabla_x (f(\tilde{x})_{j^*})$      $loss = L_{ce}(\tilde{x}, y) + \lambda * L_{attr}(\tilde{x})$     Update  $\theta$  using ( $loss$ )**end****return**  $f_\theta$ .**end**

---

[18, 23]. In the next section, we propose the formulation for our attributional robust training methodology.

### 3.2. Saliency Robustness Training

In our training methodology, given an input image  $x \in \mathbb{R}^n$  and its label  $y$ , we calculate its attribution map with respect to output logit  $i \in \{1 \dots k\}$  via  $\nabla_x f(x)_i$ . We will use  $g_i(x)$  to denote  $\nabla_x f(x)_i$  in our paper. Our aim is to make  $g_y(x)$  and classification loss landscape invariant in the local neighbourhood of  $x$  by optimizing the following objective:

$$\underset{\theta}{\text{minimize}} \mathbb{E}_{(x,y)} \left[ L_{ce}(x + \delta, y) + \max_{\delta \in B_\epsilon} L_{attr}(g_y(x + \delta)) \right] \quad (2)$$

where  $L_{ce}$  is the standard cross entropy loss and  $L_{attr}$  is the loss that encourages the alignment of  $g_y(x)$  with  $x$ . Here,  $L_{attr}$  promotes similar images to possess similar attribution maps. We take motivation from the fact that meaningful saliency maps of images are perceptually similar to image itself. We define  $L_{attr}$  as:

$$\begin{aligned} L_{attr}(x) &= \log(1 + \exp(-(d_{neg} - d_{pos}))) \\ \text{where } d_{pos} &= 1 - \cos(g_y(x), x) \\ d_{neg} &= 1 - \cos(g_{j^*}(x), x) \\ j^* &= \arg \max_{j \neq y} f(x)_j \end{aligned} \quad (3)$$

$L_{attr}$  is a soft-margin triplet loss with anchor  $x$ , its positive instance  $g_y(x)$  and its negative instance  $g_{j^*}(x)$ . The idea being that attribution map calculation with respect to different class logit value should be different and  $g_y(x)$  should have the largest perceptual similarity with the image  $x$ .

Thus, our final training methodology consists of two steps: first, we calculate a perturbed image  $\tilde{x} = x + \delta$  that maximizes  $L_{attr}$  by using iterative projected gradient descent; secondly, we use  $\tilde{x}$  as the new training point on which  $L_{ce}$  and  $L_{attr}$  is minimized. We point out that this min-max formulation is different from adversarial training [37], as only  $L_{attr}$  is maximized to calculate the perturbation  $\delta$ . Figure 2 shows the block diagram of our training approach.

The optimization of  $L_{attr}$  involves computing gradient of  $g_i(x)$  with respect to input  $x$  which suffers from the problem of vanishing second derivative in case of relu activations, i.e.  $\partial^2 f_i / \partial x^2 \approx 0$ . To alleviate this, while optimizing  $L_{attr}$ , we replace relu with softplus non-linearities [18], as it has well-defined second derivative. The softplus approximates to relu as the value of  $\beta$  increases. After the training is complete, we perform and report all our results on the model with the relu activation neural network.

$$\text{softplus}_\beta(x) = \frac{\log(1 + e^{\beta x})}{\beta} \quad (4)$$

Pseudo-code for our training methodology is given in Algorithm 1. Note that other attribution methods can also be used (e.g. Integrated gradient[59]) in our formulation of  $L_{attr}$ .

### 3.3. Connection between Robustness and Interpretability

It was shown by authors of [24, 60] that classification models are vulnerable to small imperceptible adversarial perturbations  $\delta$  which when added to  $x$  drastically changes the model's prediction. Such perturbed images are referred to as adversarial examples and are calculated by optimizing the following:

$$x_{adv} = \arg \max_{\tilde{x}: \|\tilde{x} - x\|_p < \epsilon} L_{ce}(\theta, \tilde{x}, y) \quad (5)$$

where  $L_{ce}$  is cross entropy loss and the perturbation is constrained by a  $p$  norm to ensure that the perturbed example is perceptually close to the original sample.

Recently, it was observed by Tsipras et al.[61] that an adversarially robust model has salient gradients  $g_{i^*}(x)$  i.e. saliency map highlights the perceptually relevant features of the image well and in turn looks similar to the image  $x$ . For classifiers satisfying locally affine approximation using relu activations, Etmann *et al.* [21] derive theoretical connection between adversarial robustness and the alignment of  $g_{i^*}(x)$  with image  $x$ . We can quantify adversarial robustness for  $x$  as its distance to the nearest decision boundary  $\rho(x)$ . For classifiers with sufficiently large locally affine region, we can upper bound  $\rho(x)$  by  $\tilde{\rho}$ :

$$\tilde{\rho}(x) = \min_{j \neq i^*} \frac{f_\theta(x)_{i^*} - f_\theta(x)_j}{\|g_{i^*}(x) - g_j(x)\|} \quad (6)$$

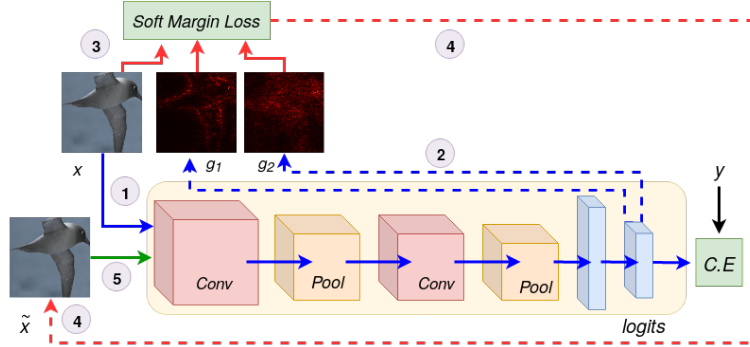


Figure 2: Block diagram summarizing our training technique for attributional robustness. Here, C.E. denotes cross entropy loss, dashed line represents the backward gradient flow and the bold lines denotes forward call in neural network.

Dataset	Approach	Saliency Robustness			Accuracy	
		IN	K	S	Natural	PGD-40 Attack
CIFAR-10	Natural	13.72,40.25	09.5,49.17	13.97,65.99	95.26	0.
	PGD-10 [37]	54.8,69.00	54.06,72.27	72.33,88.18	87.32	44.07
	Ours	<b>76.07,92.90</b>	<b>70.31,91.76</b>	<b>86.69,98.23</b>	89.84	37.58
SVHN	Natural	17.95,60.43	15.80,56.50	23.16,72.43	95.66	0.
	PGD-7 [37]	39.63,39.67	39.33,55.56	55.56,70.56	92.84	50.12
	Ours	<b>41.47,61.37</b>	<b>41.47,72.60</b>	<b>57.87,87.69</b>	95.47	43.56
GTSRB	Natural	38.79,68.74	41.34,76.48	57.63,91.33	99.43	19.9
	IG Norm [14]	-,74.81*	-,75.55*	-	97.02*	75.24*
	IG-SUM Norm [14]	-,74.04*	-,76.84*	-	95.68*	77.12*
	PGD-7 [37]	65.68,86.13	57.80,88.42	76.13,97.7	98.36	87.49
	Ours	<b>79.46,91.96</b>	<b>76.01,89.34</b>	<b>91.02,98.01</b>	98.47	84.66
Flower	Natural	20.20,38.22	34.33,56.43	48.33,74.13	93.91	0.
	IG Norm [14]	-,64.68*	-,75.91*	-	85.29*	24.26*
	IG-SUM Norm [14]	-,66.33*	-,79.74*	-	82.35*	47.06*
	PGD-7 [37]	<b>72.33,80.84</b>	<b>73.18,84.14</b>	<b>94.04,96.13</b>	92.64	69.85
	Ours	55.1,79.84	68.93, <b>84.87</b>	86.35, <b>96.27</b>	93.21	33.08

Table 1: Attributional and adversarial robustness of different approaches on various datasets. Attributional attack is similar to [14]. Similarity measures used are IN: *Top-k intersection*, K: *kendall's tau rank order correlation* and S: *Spearman Correlation*. The two values denote similarity between attribution maps based on *gradient* and *Intergrated Gradient* method. The accuracy marked with asterisk\* indicates it is taken from the original paper. We leave some accuracy as blank, as they are not reported in the original paper [14]

The index  $j$  for which the RHS of equation 6 is minimum is denoted as  $j^*$ . Etmann *et al.* proved that  $\tilde{\rho}(x)$  is upper bounded by the alignment between  $x$  and  $g_{j^*}(x)$ , i.e.

$$\begin{aligned}
 \tilde{\rho}(x) &\leq x \cdot \frac{(g_{i^*}(x) - g_{j^*}(x))}{\|g_{i^*}(x) - g_{j^*}(x)\|} + E_1 \\
 &\leq x \cdot \frac{g_{i^*}(x)}{\|g_{i^*}(x)\|} + E_2
 \end{aligned}
 \tag{7}$$

We note that the alignment of attribution maps with image  $x$  used in the formulation of  $L_{attr}$  also comes up in the above inequality.

### 3.4. Extension to Weakly supervised Object localization (WSOL)

The problem of WSOL deals with detecting objects where only class level data regarding images are available, and ground truth bounding box data is inaccessible. Generally, the pipeline for obtaining bounding box locations in WSOL relies on the attribution maps. Therefore, several methods [15, 81, 80] modify the training procedure of the classifier to obtain better attribution maps that covers the whole object in the image. Since, the aim of our training methodology is to provide robust attribution maps for the models, we think testing our proposed model in this problem setting seems relevant. Indeed, that seems to be the case as our proposed model achieves the new state-of-the-art localization results on CUB dataset.

## 4. Experiments and Results

### 4.1. Attributional and Adversarial Robustness

**Baseline** . We compare our training methodology with the following approaches:

- Natural: Standard training with minimization of cross entropy classification loss.
- PGD- $n$ : Adversarially trained model with  $n$  step PGD attack as in [37].
- IG Norm and IG-SUM Norm [14]: This is the current state-of-the-art training technique for attributional robustness that aims at making model’s integrated gradient saliency map robust.

**Implementation Details** To show the efficacy of our methodology, we benchmark on the following standard vision datasets: CIFAR-10[34], SVHN[41], GTSRB[58] and Flower [42].

For CIFAR-10, GTSRB and Flower dataset we use Wideresnet-28-10 [72] model architecture for all approaches, i.e natural, sal and PGD-10 and for SVHN dataset we use WideResNet-40-2 [72] architecture. The perturbation for our training methodology and PGD- $n$  training is  $l_\infty$  bounded with  $\epsilon = 8./255$  for all datasets. We use  $\lambda = 0.5$ ,  $\alpha = 3$  and  $\beta = 50$  for all the experiments in this paper. We use SGD optimizer while training with a step wise learning rate schedule. More details about the dataset and training can be found in the Appendix A.

**Evaluation:** To evaluate attributional robustness of models, we perform attribution attack using formulation of Ghorbani *et al.* [23] for fair comparison with [14]. The attack objective is as follows:

$$\begin{aligned} \tilde{x} = \arg \max - \sum_{k \in B} I(\tilde{x}, f(\tilde{x})_{i^*})_k \\ \text{subject to: } \|\tilde{x} - x\|_\infty < \epsilon \end{aligned} \quad (8)$$

Here,  $I(x, f(x)_{i^*})$  is the attribution map calculated using Integrated Gradient[59] method and  $B$  is the set of top- $k$  indices of attribution map of image  $x$ . We optimize for the above objective using iterative projected gradient descent method. We set  $k$  in top- $k$  as 1000 for flower dataset and 100 for the rest of the datasets following [14]. All other hyper-parameters used in evaluation are also same as [14].

**Similarity measure:** For assessing similarity between attribution map of  $x$  and  $\tilde{x}$  we use the following three metrics as metrics as mentioned in [14]: *Top-k intersection* (IN); *Kendall’s tau coefficient* (K); and *Spearman correlation* (S).

Kendall’s tau and Spearman correlation are a measure of similarity in ordering when ranked by the values and therefore are suitable metrics for attribution maps. *Top-k intersection* measures the percentage of common indices in top- $k$  values of attribution map of  $x$  and  $\tilde{x}$ .

We compare the robustness measure across different datasets and training approaches and report it in table 1. Our proposed approach achieves state of the art attributional robustness on the above explained metrics when compared with baseline and [14]. We also observe that our method shows improvement in adversarial robustness than that of naturally trained model.

#### 4.1.1 Weakly Supervised Image Localization

This task relies on the saliency map obtained from the classification model to estimate a bounding box for objects. We compare our approach with ADL[15]<sup>1</sup> on CUB dataset which has ground truth bounding box of 5794 bird images.

We adopt a similar approach as ADL for extracting bounding boxes except that we use gradient attribution map  $\nabla_x(f(x)_y)$  instead of CAM [82]. As a post-processing step, we convert the attribution map to grayscale, normalize it and then apply a mean filtering of  $3 \times 3$  kernel over it. Then a bounding box is fit over this heatmap to localize the object. We perform experiments on Resnet-50 [26] and VGG [54] architecture and report the results in Table 2. We use the same evaluation metrics as used in [15] i.e. Top-1 classification accuracy (*Top-1 Acc*): Localization accuracy when ground truth is known (*GT-Known Loc*), i.e when intersection over union (IoU) of estimated box and ground truth bounding box  $> 0.5$ ; Top-1 localization accuracy, i.e. when prediction is correct and IoU of bounding box  $> 0.5$  (*Top-1 Loc*). Model trained with our approach results in highest GT-Known Loc and Top-1 Loc for both Resnet-50 and VGG-GAP [15] model with gradient saliency method [53]. We use  $l_\infty$  bound of  $\epsilon = 2./255$  for our training methodology and PGD-7 training on CUB dataset. We also show a qualitative evaluation comparing the bounding box estimated by our approach with [15] in figure 3. More examples images are shown in Appendix A For training the models, we use a SGD optimizer with a step-wise learning rate schedule as mentioned in [15].

## 5. Discussion and Ablation Studies

To understand the scope and impact of the proposed approach, we perform various experiments and report these findings in this section. We choose CIFAR-10 as the primary dataset for the following experiments.

<sup>1</sup><https://github.com/junsukchoe/ADL/tree/master/Pytorch>

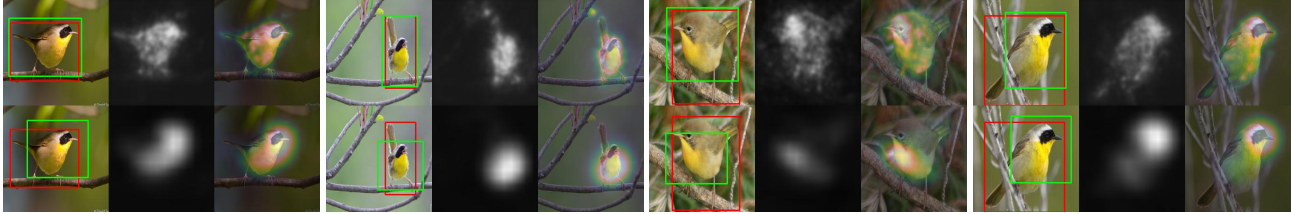


Figure 3: Comparison of heatmap and estimated bounding box by VGG model trained via our method and ADL on CUB dataset; top row corresponds to our method and bottom row corresponds to ADL. Red bounding box is ground truth and green bounding box corresponds to the estimated bo

Model	Method	Saliency Method				Top-1 Acc
		Grad		CAM		
		GT-Known Loc	Top-1 Loc	GT-Known Loc	Top-1 Loc	
ResNet50-SE	ADL[15]	-	-	-	62.29*	80.34*
ResNet50	ADL#	52.93	43.78	56.85	47.53	80.0
	Natural	50.2	42.0	60.37	50.0	81.12
	PGD-7[37]	69.93	50.10	49.82	35.38	70.02
	Ours	<b>79.89</b>	<b>63.84</b>	60.82	48.74	78.38
VGG-GAP	ADL#	63.18	43.59	69.36	50.88	70.31
	Natural	72.54	53.81	48.75	35.03	72.938
	Ours	<b>75.40</b>	<b>57.04</b>	41.75	30.35	74.51

Table 2: Weakly Supervised Localization on CUB dataset. Bold text refers to the best GT-Known Loc and Top-1 Loc for each model architecture. \* denotes directly reported from the paper. # denotes our implementation of ADL from the official code released by [15]<sup>1</sup>

Model	Saliency Method		
	Grad	IntGrad	GradCAM++
Natural	0.2441	0.3372	0.0200
PGD-7 [37]	0.2465	0.4222	<b>0.1097</b>
Ours	<b>0.3172</b>	<b>0.6038</b>	0.0849

Table 3: Results of weakly supervised segmentation on Flower dataset. Grad: Gradients; IntGrad: Integrated Gradients.

Methods	GN	SN	IN	DB	GI-B	MB	ZB	S	F
Natural	49.16	61.42	59.22	83.55	53.84	79.16	79.18	84.53	91.6
PGD-10	83.32	84.33	73.73	83.09	81.27	79.60	82.07	82.68	68.81
Ours	85.44	86.41	77.07	86.07	81.70	83.14	85.54	84.99	71.04
	B	C	E	P	J	Sp-N	GB	Sp	Sa
Natural	94.37	87.63	84.44	74.12	79.76	65.04	73.88	86.52	92.92
PGD-10	85.97	57.86	81.68	85.56	85.56	83.64	81.36	82.58	84.92
Ours	89.42	56.69	84.72	87.64	87.89	86.02	84.36	85.01	87.46

Table 4: Top-1 accuracy of different models on perturbed variants of test-set(GN:Gaussian noise; SN: Shot noise; IN: Impulse noise; DB: Defocus blur; GI-B: Glass blur; MB: Motion blur; ZB: Zoom blur; S: Snow; F: Fog; B: Brightness; C: Contrast; E: Elastic transform; P:Pixelation noise; J: Jpeg compression;Sp-N: Speckle Noise; GB: Gaussian Blur; Sp: Spatter; Sa: Saturate)

**Robustness to targeted attribution attack** In targeted attribution attack, the aim is to calculate perturbations that minimize the dissimilarity between the attribution maps of given two images. We evaluate the attributional robustness of our proposed model in targeted attribution attack setting[18] using the attribution method [59]. For getting targeted attribution map we randomly shuffle a batch of

1000 test set examples and evaluate our method and PGD-10 trained model on this set. The *kendall's tau coefficient* and *top-k intersection* similarity measure of original and perturbed image on our model was 64.76 and 70.64 as compared to 36.29 and 31.81 on PGD-10 model. The higher correlations for model trained via our approach reflects the efficacy of our approach in targeted attribution attack setting.

**Image Segmentation** Image segmentation is an important vision task for which collecting training data annotations can easily prove to be time-consuming and costly. Therefore, recent works [33, 64, 65, 30, 44, 77, 43] in weakly supervised segmentation are focusing on training models using weaker annotations like image labels instead of ground-truth segmentation masks. We show that as the model becomes robust to adversarial and attributional attacks, the saliency maps can act as a better prior for segmentation masks. We show this on flower dataset where we have access to ground-truth segmentation masks of 849 images. We evaluate our results using *Top-1 Seg* metric which is analogous to the *Top-1 Loc* metric used in weakly supervised localization in Section 4.1.1. *Top-1 Seg* considers an answer as correct when the model prediction is correct and the IoU of ground-truth mask and estimated mask is atleast 50%. We compare our approach against natural and PGD-7 trained models using three different

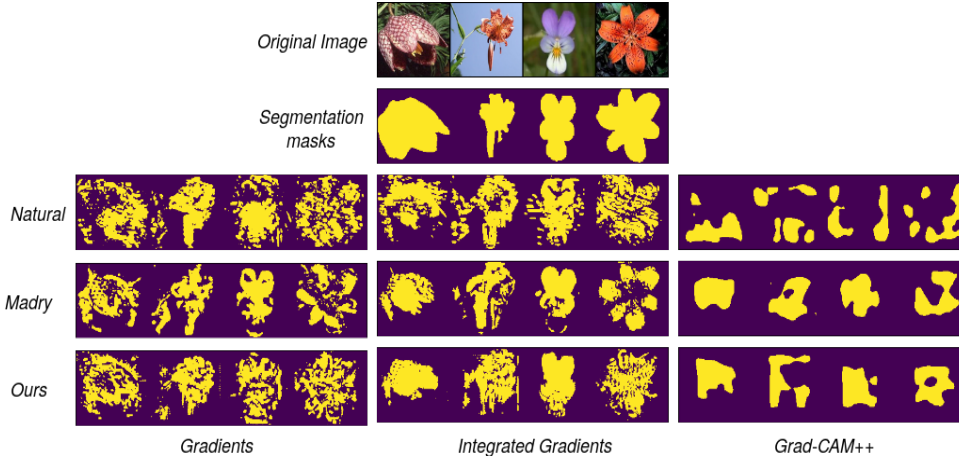


Figure 4: Example images of weakly supervised segmentation masks obtained from different models via different attribution methods

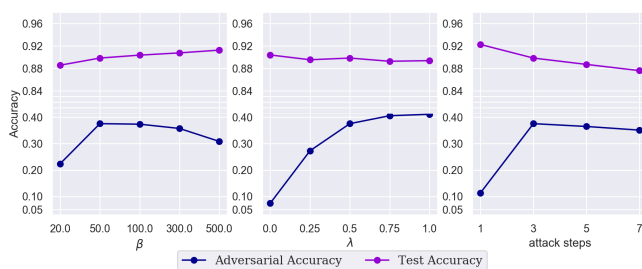


Figure 5: Test accuracy and adversarial accuracy (PGD-40 perturbations) on varying  $\beta$ ,  $\lambda$  and attack steps in our training methodology on CIFAR-10

saliency methods: gradients[53], Integrated Gradients [59] and GradCAM++[13] in table 3. Saliency maps are converted into gray-scale heatmap and a smoothing filter<sup>2</sup> is applied as a post-processing step. Example images of weakly-supervised segmentation masks generated by above models and explanation methods can be seen in figure 4. From table 3, we can see that our approach generally outperforms the Natural and Madry (PGD-7) on different attribution techniques.

**Robustness to various common perturbation [27] and spatial adversarial perturbation [20]** . We compare our proposed model with PGD-10 on the common perturbations dataset released by Hendrycks *et al.* [27] for CIFAR-10. The dataset consists of perturbed images with 75 commonplace visual perturbations at varying intensity levels. Our model achieves better generalization than other models on almost all perturbations as shown in table 4. We also perform comparison on spatial attack by Engstrom *et al.* [20] and observe robustness of 11.13% and 6.76% for our model

<sup>2</sup><https://pillow.readthedocs.io/en/5.1.x/reference/ImageFilter.html>



Figure 6: Top-k Intersection and Kendall correlation measure of attributional robustness on varying  $\beta$ ,  $\lambda$  and attack steps in our training methodology on CIFAR-10

and PGD-10 trained model respectively.

**Robustness to stronger attacks** To show the absence of gradient masking and obfuscation [10, 7], we evaluate our model on a gradient free adversarial optimization algorithm [63] and a higher iteration PGD attack. We observe similar adversarial robustness when we increase the number of steps in PGD-attack. For 100 step and 500 step PGD attack we achieve 37.42 % and 37.18 % accuracy respectively. On SPSA [63] attack our model and PGD-10 trained model obtains 46.7 and 55.61 adversarial accuracy respectively. We report the SPSA [63] attack results over 1000 random samples from test set.

**Effect of  $\beta$  and  $\lambda$  on Performance** We fix the values of  $\lambda$  to 0.5,  $a$  to 3 (best-performing values) and train the model for different values of  $\beta$ . The left plot in Fig 5 shows the influence of the  $\beta$  in the performance (i.e. Test Accuracy and Adversarial accuracy on PGD-40 perturbations) of the model. It can be observed from the plot that initially, adversarial accuracy increases with increasing  $\beta$ , but the trend reverses for higher values of  $\beta$ . However, the test accuracy





Figure 7: Qualitative examples of gradient attribution map [53] for different models on CIFAR-10. Top to bottom: Image; attribution map for Natural model; PGD-10 trained model; model trained using our approach

increases with increasing  $\beta$ . The left plot in Fig 6 shows attributional robustness of models with varying  $\beta$ . Here, we observe a similar trend that initially the attributional robustness increases till  $\beta = 100$  and then decreases. To examine the role of soft-margin triplet loss on the proposed training methodology, we fix  $\beta$  to 50,  $a$  to 3 and train the model for different values of  $\lambda$ . The hyperparameter  $\lambda$  controls the ratio of weight assigned to the classification loss and the soft-margin triplet loss. The middle plot in Fig 5 and 6 show the results of this experiment. We find that the attributional and adversarial robustness of model increases with increasing  $\lambda$  and saturates at 0.75. However, we observe that the test accuracy starts to suffer as the magnitude of  $\lambda$  increases.

**Effect of  $a$  on Performance** We analyze the effect of attribution attack steps  $a$  for our proposed training methodology. We fix  $\lambda$  to 0.5,  $\beta$  to 50 and vary attack steps  $a$  to examine the performance. We find that the performance in terms of test accuracy, adversarial accuracy and attributional robustness saturates or decreases after  $a = 3$  as showed in the right plot of Fig 5 and 6.

**Qualitative evaluation of attribution maps** We observe that the proposed model shows visually semantic attribution map obtained via [53] in figure 7. We note that, similar remarks were also made for adversarially trained models in [61].

**Attributional Robustness** In Fig 8, we show the variance box plot of attributional robustness measure on Kendall Correlation and Top-k Intersection for naturally trained, our model and adversarially trained PGD-10 [37] model. The configuration for evaluating the attributional robustness is same as mentioned in [14].

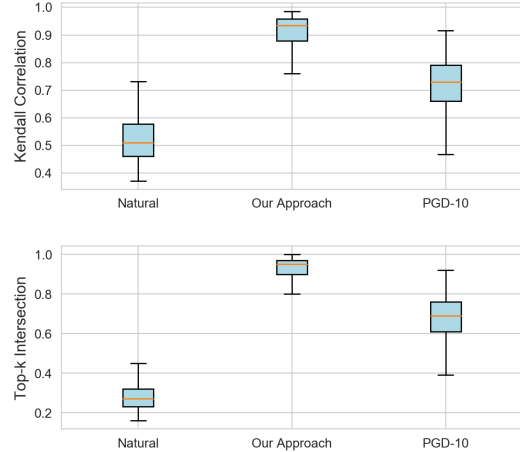


Figure 8: Variance Box Plot of Attributional Robustness measure for different models on Kendall Correlation (top) and Top-k Intersection (bottom) for 1000 test samples of CIFAR-10

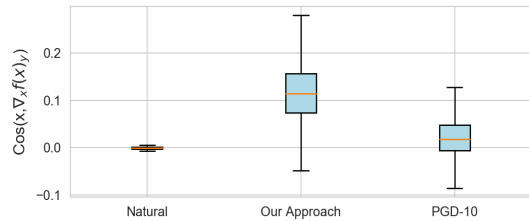


Figure 9: Cosine between  $x$  and  $\nabla_x f(x)_y$  for different models over test-set of CIFAR-10

**Evaluation of Cosine between  $x$  and  $\nabla_x f(x)_y$**  In Fig 9, we show the statistics of the cosine of  $x$  and  $\nabla_x f(x)_y$  on the test set for CIFAR-10 for different models. We observe that our proposed approach has the highest alignment between the image  $x$  and its saliency map [53]. For naturally trained model, the cosine measure is particularly low when compared with adversarially trained (PGD-10) [37] and our model.

**Using  $L_{attr} + L_{ce}$  to calculate attribution distorting examples  $\tilde{x}$**  With the motive to combine the benefits from attributional and adversarial robust model, we augment the loss function our approach with adversarial loss [37] also. We observe that the model achieves an adversarial accuracy of 52.31 with test accuracy of 85.33. However, the attributional robustness measure of Top-k intersection and kendall correlation using integrated gradients decreases to 74 and 77 from 92.9 and 91.76 respectively.

## 6. Conclusion

We observed that increasing the alignment between the input and the saliency map generated from the network's

prediction leads to improvement in the attributional robustness. We empirically showed this for both un-targeted and targeted attribution attacks over several benchmark datasets. We showed that the attributional robustness also brings out other improvements in the network, such as reduced vulnerability to adversarial attacks and common perturbations. For other vision tasks such as weakly supervised object localization and segmentation, our attributionally robust model achieves a new state-of-the-art accuracy even without being explicitly trained to achieve that objective. Furthermore, given the improvements in other vision tasks, we believe that attributional robustness is an essential area of research in computer vision domain, and we hope that our work can open a discussion around this broader notion of robustness.

## References

- [1] Julius Adebayo, Justin Gilmer, Ian Goodfellow, and Been Kim. Local explanation methods for deep neural networks lack sensitivity to parameter values. *ICLR Workshop*, 2018. [2](#)
- [2] Julius Adebayo, Justin Gilmer, Michael Muehly, Ian Goodfellow, Moritz Hardt, and Been Kim. Sanity checks for saliency maps. *NIPS*, 2018. [3](#)
- [3] Naveed Akhtar and Ajmal Mian. Threat of adversarial attacks on deep learning in computer vision: A survey. *IEEE Access*, 2018. [3](#)
- [4] Samy Bengio, Alexey Kurakin, and Ian J. Goodfellow. Adversarial examples in the physical world. *ICLR Workshop*, 2017. [3](#)
- [5] David Alvarez-Melis and Tommi S Jaakkola. On the robustness of interpretability methods. *ICML 2018 Workshop*, 2018. [2](#)
- [6] David Alvarez-Melis and Tommi S. Jaakkola. Towards robust interpretability with self-explaining neural networks. *NeurIPS*, 2018. [2](#)
- [7] Anish Athalye, Nicholas Carlini, and David Wagner. Obfuscated gradients give a false sense of security: Circumventing defenses to adversarial examples. *ICML*, 2018. [3](#), [8](#)
- [8] Sebastian Bach, Alexander Binder, Grégoire Montavon, Frederick Klauschen, Klaus-Robert Müller, and Wojciech Samek. On pixel-wise explanations for non-linear classifier decisions by layer-wise relevance propagation. *PLoS ONE* 10(7): e0130140, 2015. [2](#)
- [9] David Bau, Bolei Zhou, Aditya Khosla, Aude Oliva, and Antonio Torralba. Network dissection: Quantifying interpretability of deep visual representations. In *Computer Vision and Pattern Recognition*, 2017. [2](#)
- [10] Nicholas Carlini, Anish Athalye, Nicolas Papernot, Wieland Brendel, Jonas Rauber, Dimitris Tsipras, Ian Goodfellow, Aleksander Madry, and Alexey Kurakin. On evaluating adversarial robustness. *arXiv preprint arXiv:1902.06705*, 2019. [3](#), [8](#)
- [11] Nicholas Carlini and David Wagner. Towards evaluating the robustness of neural networks. In *2017 IEEE Symposium on Security and Privacy (SP)*, 2017. [3](#)
- [12] Chun-Hao Chang, Elliot Creager, Anna Goldenberg, , and David Duvenaud. Explaining image classifiers by adaptive dropout and generative in-filling. *arXiv preprint arXiv:1807.08024*, 2018. [2](#)
- [13] Aditya Chattopadhyay, Anirban Sarkar, Prantik Howlader, and Vineeth N Balasubramanian. Grad-cam++: Generalized gradient-based visual explanations for deep convolutional networks. *arXiv preprint arXiv:1710.11063*, 2017. [2](#), [8](#)
- [14] Jiefeng Chen, Xi Wu, Vaibhav Rastogi, Yingyu Liang, and Somesh Jha. Robust attribution regularization. *arXiv preprint arXiv:1905.09957*, 2019. [1](#), [2](#), [3](#), [5](#), [6](#), [9](#), [13](#)
- [15] Junsuk Choe and Hyunjung Shim. Attention-based dropout layer for weakly supervised object localization. In *Proceedings of the IEEE Conference on Computer Vision and Pattern Recognition*, pages 2219–2228, 2019. [3](#), [5](#), [6](#), [7](#), [14](#)
- [16] Moustapha Cisse, Piotr Bojanowski, Edouard Grave, Yann Dauphin, and Nicolas Usunier. Parseval networks: Improving robustness to adversarial examples. In *ICML*, 2017. [3](#)
- [17] Piotr Dabkowski and Yarín Gal. Real time image saliency for black box classifiers. In *NIPS*, 2017. [2](#)
- [18] Ann-Kathrin Dombrowski, Maximilian Alber, Christopher J Anders, Marcel Ackermann, Klaus-Robert Müller, and Pan Kessel. Explanations can be manipulated and geometry is to blame. *arXiv preprint arXiv:1906.07983*, 2019. [1](#), [2](#), [4](#), [7](#)
- [19] Mengnan Du, Ninghao Liu, and Xia Hu. Techniques for interpretable machine learning. *arXiv preprint arXiv:1808.00033*, 2018. [2](#)
- [20] Logan Engstrom, Brandon Tran, Dimitris Tsipras, Ludwig Schmidt, and Aleksander MÅdry. Exploring the landscape of spatial robustness. *ICML*, 2019. [3](#), [8](#)
- [21] Christian Etmann, Sebastian Lunz, Peter Maass, and Carola-Bibiane Schönlieb. On the connection between adversarial robustness and saliency map interpretability. *arXiv preprint arXiv:1905.04172*, 2019. [4](#)
- [22] Ruth C. Fong and Andrea Vedaldi. Interpretable explanations of black boxes by meaningful perturbation. In *ICCV*, 2017. [2](#)
- [23] Amirata Ghorbani, Abubakar Abid, and James Zou. Interpretation of neural networks is fragile. In *Proceedings of the AAAI Conference on Artificial Intelligence*, volume 33, pages 3681–3688, 2019. [1](#), [2](#), [3](#), [4](#), [6](#)
- [24] Ian J. Goodfellow, Jonathon Shlens, and Christian Szegedy. Explaining and harnessing adversarial examples. In *International Conference on Learning Representations*, 2015. [1](#), [4](#)
- [25] Ian J. Goodfellow, Jonathon Shlens, and Christian Szegedy. Explaining and harnessing adversarial examples. *ICLR*, 2015. [3](#)
- [26] Kaiming He, Xiangyu Zhang, Shaoqing Ren, and Jian Sun. Deep residual learning for image recognition. *arXiv preprint arXiv:1512.03385*, 2015. [6](#), [14](#)
- [27] Dan Hendrycks and Thomas Dietterich. Benchmarking neural network robustness to common corruptions and perturbations. *Proceedings of the International Conference on Learning Representations*, 2019. [8](#)

- [28] Andrew Ilyas, Logan Engstrom, Anish Athalye, and Jessy Lin. Black-box adversarial attacks with limited queries and information. *ICML*, 2018. 3
- [29] Daniel Jakubovitz and Raja Giryes. Improving dnn robustness to adversarial attacks using jacobian regularization. *ECCV*, 2018. 3
- [30] Jiang, Olamide Tawose, Pei, Zhilong Wang, and Zhao. Weakly-supervised image semantic segmentation based on superpixel region merging. *Big Data and Cognitive Computing*, 3:31, 06 2019. 7
- [31] Been Kim, Martin Wattenberg, Justin Gilmer, Carrie Cai, James Wexler, Fernanda Viegas, and Rory Sayres. Interpretability beyond feature attribution: Quantitative testing with concept activation vectors (tcav). *ICML*, 2018. 2
- [32] Pang Wei Koh and Percy Liang. Understanding black-box predictions via influence functions. In Doina Precup and Yee Whye Teh, editors, *Proceedings of the 34th International Conference on Machine Learning*, volume 70 of *Proceedings of Machine Learning Research*, pages 1885–1894, International Convention Centre, Sydney, Australia, 06–11 Aug 2017. PMLR. 2
- [33] Alexander Kolesnikov and Christoph H. Lampert. Seed, expand and constrain: Three principles for weakly-supervised image segmentation. *CoRR*, abs/1603.06098, 2016. 7
- [34] Alex Krizhevsky, Vinod Nair, and Geoffrey Hinton. Cifar-10. URL <http://www.cs.toronto.edu/kriz/cifar.html>, 2010. 6, 13
- [35] Anish Athalye Logan Engstrom, Andrew Ilyas. Evaluating and understanding the robustness of adversarial logit pairing. *NeurIPS SECML*, 2018. 3
- [36] Chunchuan Lyu, Kaizhu Huang, and Hai-Ning Liang. A unified gradient regularization family for adversarial examples. *ICDM*, 2015. 3
- [37] Aleksander Madry, Aleksandar Makelov, Ludwig Schmidt, Dimitris Tsipras, and Adrian Vladu. Towards deep learning models resistant to adversarial attacks. *arXiv preprint arXiv:1706.06083*, 2017. 3, 4, 5, 6, 7, 9, 13, 14
- [38] MadryLab. cifar10\_challenge. URL [https://github.com/MadryLab/cifar10\\_challenge](https://github.com/MadryLab/cifar10_challenge), 2017. 13
- [39] Seyed-Mohsen Moosavi-Dezfooli, Alhussein Fawzi, and Pascal Frossard. Deepfool: a simple and accurate method to fool deep neural networks. *arXiv preprint arXiv:1511.04599v3*, 2016. 3
- [40] Seyed-Mohsen Moosavi-Dezfooli, Alhussein Fawzi, Jonathan Uesato, and Pascal Frossard. Robustness via curvature regularization, and vice versa. *CVPR*, 2019. 3
- [41] Yuval Netzer, Tao Wang, Adam Coates, Alessandro Bisacco, Bo Wu, and Andrew Y. Ng. Reading digits in natural images with unsupervised feature learning. In *NIPS Workshop on Deep Learning and Unsupervised Feature Learning 2011*, 2011. 6, 13
- [42] Maria-Elena Nilsback and Andrew Zisserman. A visual vocabulary for flower classification. In *IEEE Conference on Computer Vision and Pattern Recognition*, volume 2, pages 1447–1454, 2006. 6, 13
- [43] Maria-Elena Nilsback and Andrew Zisserman. Delving deeper into the whorl of flower segmentation. *Image Vision Comput.*, 28(6):1049–1062, June 2010. 7
- [44] Seong Joon Oh, Rodrigo Benenson, Anna Khoreva, Zeynep Akata, Mario Fritz, and Bernt Schiele. Exploiting saliency for object segmentation from image level labels. *CoRR*, abs/1701.08261, 2017. 7
- [45] Nicolas Papernot, Patrick McDaniel, Ian J. Goodfellow, Somesh Jha, Z. Berkay Celik, and Ananthram Swami. Practical black-box attacks against machine learning. *ACM*, 2017. 3
- [46] Vitali Petsiuk, Abir Das, and Kate Saenko. Rise: Randomized input sampling for explanation of black-box models. In *BMVC*, 2018. 2
- [47] Chongli Qin, James Martens, Sven Gowal, Dilip Krishnan, Alhussein Fawzi, Soham De, Robert Stanforth, Pushmeet Kohli, et al. Adversarial robustness through local linearization. *arXiv preprint arXiv:1907.02610*, 2019. 3
- [48] Marco Tulio Ribeiro, Sameer Singh, and Carlos Guestrin. Why should i trust you?: Explaining the predictions of any classifier. In *ACM SIGKDD*, 2016. 2
- [49] Andrew Slavin Ross and Finale Doshi-Velez. Improving the adversarial robustness and interpretability of deep neural networks by regularizing their input gradients. *AAAI*, 2018. 3
- [50] Ramprasaath R. Selvaraju, Abhishek Das, Ramakrishna Vedantam, Michael Cogswell, Devi Parikh, and Dhruv Batra. Grad-cam: Visual explanations from deep networks via gradient-based localization. 2016. 2
- [51] Avanti Shrikumar, Peyton Greenside, and Anshul Kundaje. Learning important features through propagating activation differences. pages 3145–3153, 2017. 2
- [52] Avanti Shrikumar, Peyton Greenside, Anna Shcherbina, and Anshul Kundaje. Not just a black box: Learning important features through propagating activation differences. *arXiv preprint arXiv:1605.01713*, 2016. 2
- [53] Karen Simonyan, Andrea Vedaldi, and Andrew Zisserman. Deep inside convolutional networks: Visualising image classification models and saliency maps. *arXiv preprint arXiv:1312.6034*, 2013. 2, 6, 8, 9, 14
- [54] Karen Simonyan and Andrew Zisserman. Very deep convolutional networks for large-scale image recognition. *arXiv preprint arXiv:1409.1556*, 2014. 6
- [55] Abhishek Sinha, Mayank Singh, Nupur Kumari, Balaji Krishnamurthy, Harshitha Machiraju, and VN Balasubramanian. Harnessing the vulnerability of latent layers in adversarially trained models. *arXiv preprint arXiv:1905.05186*, 2019. 3
- [56] Daniel Smilkov, Nikhil Thorat, Been Kim, Fernanda Viégas, and Martin Wattenberg. Smoothgrad: removing noise by adding noise. *Workshop on Visualization for Deep Learning, ICML*, 2017. 2
- [57] Jost Tobias Springenberg, Alexey Dosovitskiy, Thomas Brox, and Martin Riedmiller. Striving for simplicity: The all convolutional net. *ICLR workshop*, 2015. 2
- [58] Johannes Stallkamp, Marc Schlipsing, Jan Salmen, and Christian Igel. The German Traffic Sign Recognition Benchmark: A multi-class classification competition. In *IEEE International Joint Conference on Neural Networks*, pages 1453–1460, 2011. 6, 13
- [59] Mukund Sundararajan, Ankur Taly, and Qiqi Yan. Axiomatic attribution for deep networks. *ICML*, 2017. 1, 2, 3, 4, 6, 7, 8

- [60] Christian Szegedy, Wojciech Zaremba, Ilya Sutskever, Joan Bruna, Dumitru Erhan, Ian J. Goodfellow, and Rob Fergus. Intriguing properties of neural networks. *ICLR*, 2014. 1, 4
- [61] Dimitris Tsipras, Shibani Santurkar, Logan Engstrom, Alexander Turner, and Aleksander Madry. Robustness may be at odds with accuracy. In *ICLR*, 2019. 4, 9
- [62] Yusuke Tsuzuku, Issei Sato, and Masashi Sugiyama. Lipschitz-margin training: Scalable certification of perturbation invariance for deep neural networks. *NeurIPS*, 2018. 3
- [63] Jonathan Uesato, Brendan O’Donoghue, Pushmeet Kohli, and Aaron van den Oord. Adversarial risk and the dangers of evaluating against weak attacks. *ICML*, 2018. 3, 8
- [64] M. Vasconcelos, N. Vasconcelos, and G. Carneiro. Weakly supervised top-down image segmentation. In *2006 IEEE Computer Society Conference on Computer Vision and Pattern Recognition (CVPR’06)*, volume 1, pages 1001–1006, June 2006. 7
- [65] A. Vezhnevets and J. M. Buhmann. Towards weakly supervised semantic segmentation by means of multiple instance and multitask learning. In *2010 IEEE Computer Society Conference on Computer Vision and Pattern Recognition*, pages 3249–3256, June 2010. 7
- [66] Jörg Wagner, Jan Mathias Köhler, Tobias Gindele, Leon Hetzel, Jakob Thaddä us Wiedemer, and Sven Behnke. Interpretable and fine-grained visual explanations for convolutional neural networks. In *CVPR*, 2019. 2
- [67] C. Wah, S. Branson, P. Welinder, P. Perona, and S. Belongie. The Caltech-UCSD Birds-200-2011 Dataset. Technical Report CNS-TR-2011-001, California Institute of Technology, 2011. 14
- [68] Chaowei Xiao, Jun-Yan Zhu, Bo Li, Warren He, Mingyan Liu, and Dawn Song. Spatially transformed adversarial examples. *ICLR*, 2018. 3
- [69] Kaidi Xu, Sijia Liu, Pu Zhao, Pin-Yu Chen, Huan Zhang, Quanfu Fan, Deniz Erdogmus, Yanzhi Wang, and Xue Lin. Structured adversarial attack: Towards general implementation and better interpretability. *ICLR*, 2019. 3
- [70] Chih-Kuan Yeh, Joon Sik Kim, Ian E.H. Yen, and Pradeep Ravikumar. Representer point selection for explaining deep neural networks. *NIPS*, 2018. 2
- [71] Xiaoyong Yuan, Pan He, Qile Zhu, and Xiaolin Li. Adversarial examples: Attacks and defenses for deep learning. *IEEE transactions on neural networks and learning systems*, 2019. 3
- [72] Sergey Zagoruyko and Nikos Komodakis. Wide residual networks. *CoRR*, abs/1605.07146, 2016. 6, 13
- [73] Matthew D. Zeiler and Rob Fergus. Visualizing and understanding convolutional networks. In *ECCV*, 2014. 2
- [74] Haichao Zhang and Jianyu Wang. Defense against adversarial attacks using feature scattering-based adversarial training. In *NeurIPS*, 2019. 3
- [75] Hongyang Zhang, Yaodong Yu, Jiantao Jiao, Eric P. Xing, Laurent El Ghaoui, and Michael I. Jordan. Theoretically principled trade-off between robustness and accuracy. *arXiv preprint arXiv:1901.08573*, 2019. 3
- [76] Jianming Zhang, Zhe Lin, Jonathan Brandt, Xiaohui Shen, and Stan Sclaroff. Top-down neural attention by excitation backprop. *ECCV*, 2016. 2
- [77] L. Zhang, M. Song, Z. Liu, X. Liu, J. Bu, and C. Chen. Probabilistic graphlet cut: Exploiting spatial structure cue for weakly supervised image segmentation. In *2013 IEEE Conference on Computer Vision and Pattern Recognition*, pages 1908–1915, June 2013. 7
- [78] Quanshi Zhang and Song-Chun Zhu. Visual interpretability for deep learning: a survey. *arXiv preprint arXiv:1802.00614*, 2018. 2
- [79] Xinyang Zhang, Ningfei Wang, Hua Shen, Shouling Ji, Xipapu Luo, and Ting Wang. Interpretable deep learning under fire. *arXiv preprint arXiv:1812.00891*, 2018. 2
- [80] Xiaolin Zhang, Yunchao Wei, Jiashi Feng, Yi Yang, and Thomas Huang. Adversarial complementary learning for weakly supervised object localization. In *IEEE CVPR*, 2018. 5
- [81] Xiaolin Zhang, Yunchao Wei, Guoliang Kang, Yi Yang, and Thomas Huang. Self-produced guidance for weakly-supervised object localization. In *European Conference on Computer Vision*. Springer, 2018. 5
- [82] Bolei Zhou, Aditya Khosla, Agata Lapedriza, Aude Oliva, and Antonio Torralba. Learning deep features for discriminative localization. In *CVPR*, 2016. 2, 3, 6

# Appendix

## A. Attributional Robustness: Dataset and Implementation Details

In this section, we describe the datasets and model hyperparameters used in attributional robustness experiments.

**SVHN [41]:** Data and Model: SVHN consists of images of digits obtained from house numbers in Google Street View images, with 73257 digits for training and 26032 digits for testing over 10 classes. We perform experiments on SVHN using WideResNet-40-2 [72] architecture for training on reported approaches.

Hyperparameters for Training:

*Natural:* We use SGD optimizer with an initial learning rate of 0.1, momentum of 0.9,  $l_2$  weight decay of  $2e-4$  and batch size of 128. We train it for 200 epochs with a learning rate schedule decay of 0.1 at 50<sup>th</sup>, 80<sup>th</sup> and 0.5 at 150<sup>th</sup> epoch.

*PGD-7[37]:* We use the training configuration as mentioned in (cifar-10 challenge) to perform 7-step adversarial training with  $\epsilon = 8./255$ .

*Our Approach:* We use the same training configuration as mentioned in *Natural* model with  $\beta = 50$  and  $\lambda = 0.5$ . We calculate  $\tilde{x}$  using  $\epsilon = 8./255$  and  $a = 3$ .

**CIFAR-10 [34]** Data and Model: It consists of 50000 training images for 10 classes with resolution of  $32 \times 32 \times 3$ . We normalize the images with its mean and standard deviation for training. We train a WideResNet28-10 [72] model for all the experiments on this dataset.

Hyperparameters for Training:

*Natural:* We use SGD optimizer with an initial learning rate of 0.1, momentum of 0.9,  $l_2$  weight decay of  $2e-4$  and batch size of 128. We train it for 200 epochs with a learning rate schedule decay of 0.1 at 50<sup>th</sup>, 80<sup>th</sup> and 0.5 at 150<sup>th</sup> epoch.

*PGD-10[37]:* We use the training configuration as mentioned in [38] to perform 10-step adversarial training with  $\epsilon = 8./255$ .

*Our Approach:* We use the same training configuration as mentioned in *Natural* model with  $\beta = 50$  and  $\lambda = 0.5$ . We calculate  $\tilde{x}$  using  $\epsilon = 8./255$  and  $a = 3$ .

**GTSRB [58]:** Data and Model: German Traffic Signal Recognition Benchmark [58] consists of 43 classes of traffic signals with 34,799 training images, 4,410 validation images and 12,630 test images. We resize the images to  $32 \times 32 \times 3$  and normalize the images with its mean and standard deviation for training. To balance the number of

images for each class, we use data augmentation techniques consisting of rotation, translation, and projection transforms to extend the training set to 10,000 images per class as in [14]. We train WideResNet28-10 [72] model for carrying out experiments related to this dataset.

Hyperparameters for Training:

*Natural:* We use SGD optimizer with an initial learning rate of 0.1, momentum of 0.9,  $l_2$  weight decay of  $2e-4$  and batch size of 128. We train it for 12 epochs with a learning rate schedule decay of 0.1 at 4<sup>th</sup>, 6<sup>th</sup> and 0.5 at 10<sup>th</sup> epoch.

*PGD-7[37]:* We use the training configuration as mentioned in (cifar-10 challenge) to perform 10-step adversarial training with  $\epsilon = 8./255$ .

*IG Norm and IG-Sum Norm [14]:* We report the accuracy as mentioned in the paper [14].

*Our Approach:* We use the same training configuration as mentioned in *Natural* model with  $\beta = 50$  and  $\lambda = 0.5$ . We calculate  $\tilde{x}$  using  $\epsilon = 8./255$  and  $a = 3$ .

**Flower [42]:** Data and Model: It is a 17 category flower dataset with 80 images for each class. We resize the images to  $128 \times 128 \times 3$  and normalize it with its mean and standard deviation for training. The training set consists of 1,224 images with 72 images per class. The test set comprises of 136 images with 8 images per class. We use standard data augmentation techniques of rotation, translation, and projection transforms to extend the training data so that each class contains 1,000 training examples as proposed in [14]. We use WideResNet28-10 [72] model for the reported approaches.

Hyperparameters for Training:

*Natural:* We use SGD optimizer with an initial learning rate of 0.1, momentum of 0.9,  $l_2$  weight decay of  $2e-4$  and batch size of 128. We train it for 68 epochs with a learning rate schedule decay of 0.1 at 15<sup>th</sup>, 35<sup>th</sup> and 0.5 at 50<sup>th</sup> epoch.

*PGD-7[37]:* We use the training configuration as mentioned in (cifar-10 challenge) to perform 7-step adversarial training with  $\epsilon = 8./255$ .

*IG Norm and IG-Sum Norm [14]:* We report the accuracy as mentioned in the paper [14].

*Our Approach:* We use the same training configuration as mentioned in *Natural* model with  $\lambda = 0.5$  and  $\beta = 50$ . We calculate  $\tilde{x}$  using  $\epsilon = 8./255$  and  $a = 3$ .

## B. Weakly Supervised Localization: Dataset and Implementation Details

In this section, we provide details of the dataset and model hyper-parameters used for the results presented in

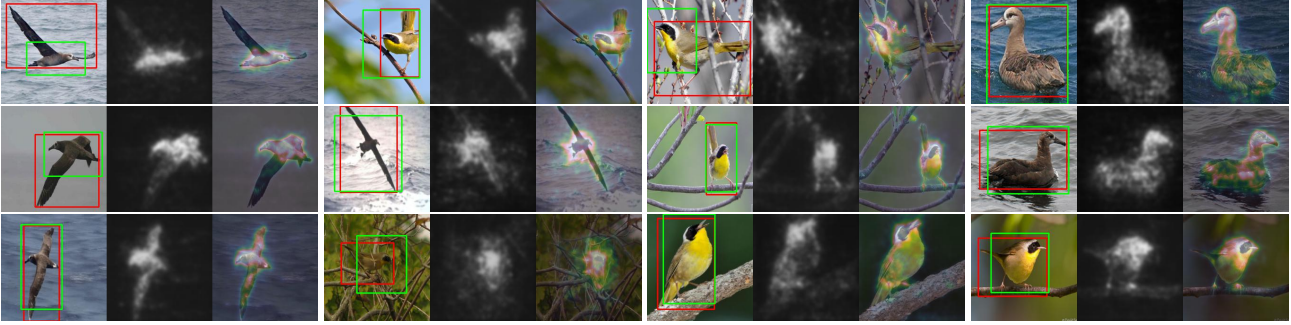


Figure 10: Examples of estimated bounding box and heatmap by ResNet50 model trained via our approach on randomly chosen images of CUB dataset; Red bounding box is ground truth and green bounding box corresponds to the estimated box

the main paper.

**Dataset and Model:** **CUB** [67] is an image dataset of 200 different bird species (mostly North American) with 11, 788 images in total. The information as a bounding box around each bird is also available. We finetune a ResNet-50 [26] model pretrained on ImageNet for the reported approaches as in [15].

**Hyper-parameters for training**

*Natural:* We use SGD optimizer with an initial learning rate of 0.01, momentum of 0.9 and  $l_2$  weight decay of  $1e-4$ . We train the model for 200 epochs with learning rate decay of 0.1 at every 60 epochs.

*PGD-7* [37]: We use same hyper-parameters as natural training with  $\epsilon = 2./255$ . and  $step\_size = 0.5/255$ . for calculating adversarial examples.

*Our Approach:* We use SGD optimizer with an initial learning rate of 0.01, momentum of 0.9 and  $l_2$  weight decay of  $2e-4$ . We decay the learning rate by 0.1 at every 40 epoch till 200 epochs. While calculating  $L_{attr}$  loss, we took mean over channels of images and gradients. Values of other hyper-parameters are  $\epsilon = 2./255$ ,  $step\_size = 1.5/255$ ,  $a = 3$ ,  $\lambda = 0.5$  and  $\beta = 50$ .

## B.1. Qualitative analysis

Fig 10 shows the estimated bounding box and heatmap derived from gradient based attribution [53] on randomly sampled images for ResNet50 model trained via our approach. From the figure 10, we observe that the estimated bounding box sometimes does not capture the object in cases where birds have extended wings, or the bird is in an occluded area with branches and twigs.